JOURNAL OF AGRICULTURAL AND FOOD CHEMISTRY

Molecular Orbital Basis for Yellow Curry Spice Curcumin's Prevention of Alzheimer's Disease

KRISHNAN BALASUBRAMANIAN†

Chemistry and Material Science Directorate, University of California, Lawrence Livermore National Laboratory, Livermore, California 94550; Department of Mathematics and Computer Science, California State University, East Bay, Hayward, California 94542; and Glenn T. Seaborg Center, Lawrence Berkeley Laboratory, University of California, Berkeley, California 94720

It is demonstrated by using high-level ab initio computations that the yellow curcumin pigment, bis-(4-hydroxy-3-methoxyphenyl)-1,6-diene-3,5-dione, in the east Indian root plant turmeric (*Curcuma longa*) exhibits unique charge and bonding characteristics that facilitate penetration into the blood−brain barrier and binding to amyloid β (Aβ). Alzheimer's disease is caused by Aβ accumulation in the brain cells combined with oxidative stress and inflammation. Consistent with the recent experimental work by Cole and co-workers (Yang, F., et al. *J. Biol. Chem.* **2004**, *280*, 5892−5901) that demonstrates curcumin pigment's binding ability to Aβ both in vivo and in vitro, it is shown here that curcumin possesses suitable charge and bonding features to facilitate the binding to Aβ. In addition, curcumin's anti-inflammatory and antioxidant properties are also attributed to electronic and structural features. It is shown that the presence of an enolic center and two phenolic polar groups separated by an essentially hydrophobic bridge of a conjugated network provides both hydrophobic and hydrophilic features to the curcumin pigment, thereby facilitating penetration into the blood−brain barrier through the former property and then binding to Aβ oligomer through the latter property. Both density functional and Møller−Plesset perturbation (MP2) computations have been carried out on the curcumin pigment to obtain fully optimized geometries in the gas phase and aqueous solution and also the atomic charges. Different isomers (keto and enol forms) have been considered to show that the enol form is the most favored and has all of the properties for an ideal antioxidant with also features to penetrate the blood−brain barrier and to bind to Aβ. This is demonstrated with natural bond charges, highest occupied and lowest unoccupied molecular orbitals, dipole moments, and Laplacian plots. The computed ionization potential and electron affinity show that curcumin has a low molecular hardness and thus has a propensity to dissociate its phenolic −OH, and the resulting charge undergoes delocalization throughout the structure, resulting in excitonic features. This feature seems to be also important for its binding capability to human proteins such as human serum albumin and Aβ.

KEYWORDS: Curcumin; molecular orbital studies; charges; polar and hydrophobic features

INTRODUCTION

The yellow food color in many Indian curry preparations is attributed to curcumin, a natural product pigment found in the east Indian root plant turmeric (*Curcuma longa*), which is used extensively in traditional Indian cooking recipes, traditional Indian cosmetics, and ayurvedic herbal remedies in larger doses (*1*−*24*). In the most commonly accepted form, the chemical structure consists of two conjugated backbones each with a ketone and a $-CH_2$ group separating the backbones and a terminal meta-methoxy-para-hydroxy phenyl ring on each side. The structure could explain (*20*) how food-flavoring agents such as vanilla, that is, 3-methoxy-4-hydroxybenzaldehyde, can be derived from turmeric through chemical conversion upon addition of acidified $KMnO_4$.

A recent experimental study by Cole and co-workers (*1*) has demonstrated that the yellow curcumin pigment in turmeric prevents and may even be a cure for Alzheimer's disease (AD). Cole and co-workers' (*1*) showed that curcumin injected peripherally in vivo into aged Tg mice crossed the blood−brain barrier and bound to amyloid B (Aβ) plaques. Cole and co-workers (*1*) fed curcumin to aged Tg2576 mice with advanced amyloid accumulation, and it was revealed that curcumin reduced amyloid levels and plaque formation decisively. Consequently, Cole and co-workers (*1*) hypothesized that curcumin directly binds to small β-amyloid species, thus inhibiting aggregation and fibril formation both in vitro and in vivo. These data suggest that curcumin effectively disaggregates Aβ and thus provide support for the use of curcumin in clinical trials to treat AD.

† E-mail balu@llnl.gov; telephone (925) 422-4984.

10.1021/jf0603533 CCC: $33.50
Published on Web 04/20/2006

Although the exact nature of its role in preventing AD is not fully understood, there is ample experimental evidence (*1*, *4*−*6*) that curcumin binds to amyloid β oligomer, the key agent that promotes plaque in the brain cell, leading to AD. It is generally understood that Aβ accumulation, oxidative damage, and inflammation of the brain cell causes AD. The yellow curcumin pigment in turmeric binds to Aβ oligomer, as curcumin seems to have all of the vital features required to penetrate the blood−brain barrier and yet possesses polar groups so as to bind to Aβ oligomer.

A number of studies (*7*−*13*) have shown that curcumin can be a prevention agent and a chemotherapeutic agent for colon cancer. Curcumin is also well-known for its anti-inflammatory and antioxidant properties, and other properties as demonstrated by a number of studies (*14*−*19*). Curcumin prevents the development of colon tumors as demonstrated in rats treated with colon carcinogen (*9*, *13*). Curcumin is also known to be a chemopreventive agent in malignant human oral epithelial cells (*11*). Several experimental studies have revealed that curcumin is a chemopreventive agent particularly for skin, oral, intestinal, and colon carcinogenesis (*8*−*13*). In many of these applications, the antioxidative and anti-inflammatory properties of curcumin are pivotal to the prevention or treatment of the disease.

Curcumin exhibits radical scavenging activity, phototoxicity to several species of bacteria under aerobic conditions, and fungicidal properties (*8*, *14*, *15*). Curcumin shows high reactivity toward peroxyl radicals and its analogues, and thus curcumin can act as a free radical scavenger. Curcumin's spectroscopy and photochemistry are quite interesting (*5*, *14*, *17*, *20*, *21*). Curcumin and its analogues seem to exhibit altered potencies against HIV-1 integrase (*24*).

Among all of the well-known properties of curcumin, the most recent finding (*1*) that it can prevent or cure AD is the most spectacular. This is mainly because brain chemistry is difficult to understand, and very few agents can penetrate the blood−brain barrier and also act as a prevention or cure of AD. The other known agents are nonsteroidal anti-inflammatory drugs (NSADs) (*2*) and congo red (*1*), although the latter is known to be toxic and its charged character is not well suited for penetration into the blood−brain barrier. Thus, it is important to understand the molecular basis and mechanism of curcumin's AD prevention or cure so that other drugs can be discovered through molecular similarity and QSAR (*25*, *26*). It is not clear as to what features of curcumin make it a dual agent; on the one hand, its hydrophobic capability facilitates penetration of the blood−brain barrier, and on the other hand, it possesses polar binding features—exhibiting duality of hydrophobicity and partly polar, thus in part being hydrophilic. It is also not clearly understood as to which features of curcumin facilitate its binding to β-amyloid or if it is a polymer of β-amyloid that curcumin binds to. There is also a question as to whether a metal ion that could enhance AD is chelated with curcumin, thus preventing AD (*1*). As more experimental and medicinal studies are carried out, it is important to understand the structural features of curcumin that lead to these ambivalent hydrophobic and hydrophilic behaviors, bonding characteristics, and so on.

The objective of this study is high-level ab initio computational study of several forms of curcumin employing large basis sets that include 801 basis functions. Accurate quantum chemical studies employing both DFT and MP2 studies on curcumin both in the gas phase and in aqueous medium have been carried out with the objective of finding the equilibrium structure, charge, bonding characteristics, and nature of the molecular orbitals, particularly the highest occupied and lowest unoccupied that are important for binding. Structural features of curcumin that facilitate penetration of the blood−brain barrier and binding to the β-amyloid have been identified here. There are a few semiempirical and ab initio studies (*20*−*23*) that employed smaller basis sets and lower levels of theory compared to the one used here. The first theoretical study on a model compound reminiscent of curcumin was carried out by the author (*20*, *21*) to understand the observed UV−visible spectra. However, there are no molecular studies that clearly demonstrate curcumin's cause for the prevention of AD. Thus, this study was carried out at a high level of theory and could result in the discovery of other species that have molecular similarities to curcumin, thus resulting in improved or new drugs for the cure or prevention of AD.

COMPUTATIONAL METHODS

Equilibrium geometries in the gaseous phase were optimized using the DFT (*28*) and second-order Møller−Plesset perturbation (MP2) (*29*). The DFT approach utilized Becke's (*29*) three-parameter hybrid functional known as B3LYP. A fairly large basis set with two sets of polarization functions denoted the 6311-G(2d,2p) basis was used, which resulted in a total of 801 contracted Gaussian functions for curcumin. Although aug-cc-pvdz basis sets are comparable in size, convergence was difficult to accomplish, and thus the 6311-G(2d,2p) basis sets have been used uniformly for all species considered here. The computations were carried out in C_1 symmetry (that is, no symmetry) to facilitate full rearrangement and relaxation of the structure to the most stable form. Thus, it was ensured that the computed minima have all real vibrational frequencies using second derivatives, establishing the structures to be true minima.

The optimized curcumin structure was placed in water to study changes to the geometry and charges in water at the DFT/B3LYP by using the self-consistent reaction field models in which the solvent was treated to be a dielectric continuum. Integral equation formalism PCM model (IEFPCM) (*31*−*33*) was used for this purpose. The geometries were fully optimized using these models to seek their structures in the aqueous medium. In the IEFPCM model, the solute is embedded in a shape-adapted cavity defined by interlocking spheres centered on each solute atom or group and with standard united atomic topological model (UATM) radii. As discussed in the next section, several isomers of curcumin have been considered, among which the primary ones are the diketo form and an enol form both in solution and in the gas phase. It should also be mentioned that other structures displayed earlier in the literature (*5*, *22*, *23*) are not plausible for the ground or low-lying states of curcumin. In the work of Zsila et al. (*5*), the $-OCH_3$ groups are on the same side as the diketo groups. This isomer is simply a rotation of the benzene ring around the bond that connects to the remaining chain. However, it is found here that this isomer is considerably higher in energy. Note that both of the isomers in the diketone form of curcumin have the $-OCH_3$ groups in the third position and $-OH$ groups in the fourth position, but the $-OCH_3$ groups are on the opposite side of the diketo or enol part of the structure. The latter isomer is much higher in energy, and thus it cannot be the ground state of curcumin in either keto or enol form. Note that even in the diketo form, the anti (trans) structure in which half of curcumin rotated around the $-CH_2$ group relative to the other half is more stable than the syn (cis) structure. Likewise, Sun et al. (*23*) have displayed a set of structures for curcumin in Figure 1 of their paper, where the $-OH$ groups are in third and the OCH_3 groups are in fourth positions. These representations are not consistent with curcumin's structure, which has $-OH$ groups in the fourth or para positions and $-OCH_3$ groups in the meta positions relative to the ring connection to the aliphatic chain.

All of the calculations were carried out using the Gaussian 03 package of codes (*34*). Geometry optimization and frequency calculations at the MP2 and DFT levels were performed on Lawrence Livermore's uv machine, which consists of 992 IBM SP4 processors as well as a server with 4 Intel IA-64 processors. The MP2 optimization consumed ~176 GB of hard drive space and several days of computing

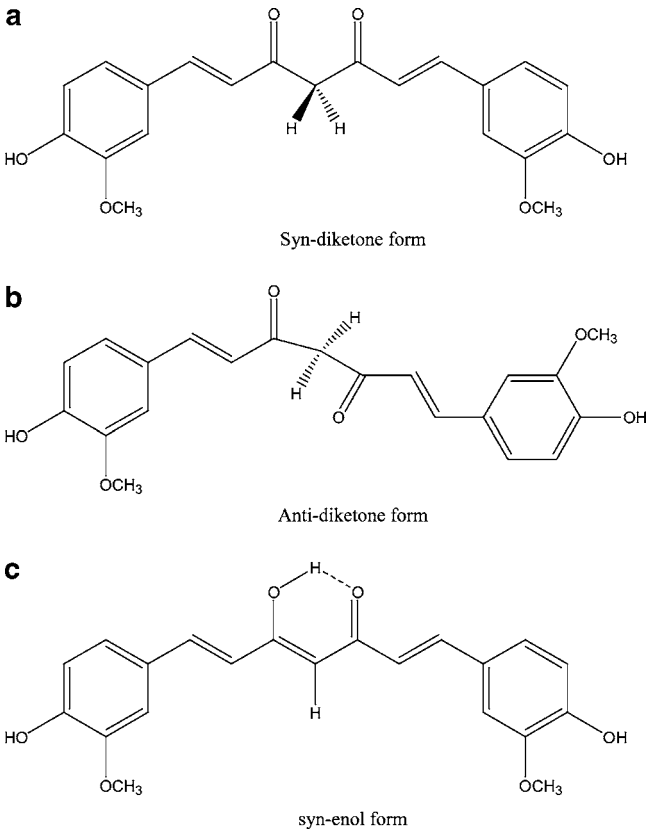

Figure 1. Two-dimensional chemical structures of syn-diketo curcumin (**a**), anti-diketo curcumin (**b**), and enolic curcumin (**c**).

time. The orbitals and charges were visualized using the Gauss View package.

RESULTS AND DISCUSSION

Curcumin's chemical structure in simple two-dimensional notation is shown in **Figure 1**. As seen from **Figure 1**, this structure has two keto groups separated by a $-CH_2$ group and a set of conjugated bonds ending with a phenyl ring with 3-methoxy-4-hydroxy substituents. However, there is recent compelling experimental and theoretical evidence that an enol structure is favored due to hydrogen bonding in the keto form, thus favoring a keto−enol tautomeric rearrangement. The aromaticity of curcumin and its ability to extend its conjugation under alkaline conditions as well as the acidic nature of phenolic −OH groups are of interest in the general context of aromaticity and other polycyclic aromatic species (*27*).

Three possible isomeric structures of curcumin that have primarily been considered are shown on **Figure 1**. In addition, some of the structures from the earlier papers were considered and were ruled out as candidates for the ground state of curcumin. The first structure shown in **Figure 1** is the most common representation of curcumin, which is called the syn-diketo form. In this form the two keto groups are on the same side, and likewise the $-OCH_3$ groups are also on the same side. Geometry optimization starting with the syn-diketo structure did not produce a minimum, and it rearranged to the anti-diketo form shown in **Figure 1** (second structure). Not only was the structure optimized with 6311-G(2d,2p) basis, but also the vibrational frequencies for the anti-diketo form were computed. The anti-diketo isomer was found to be a minimum with all real vibrational frequencies, confirming this as a potential isomer of curcumin. Note that the isomerization from the syn to the anti structure is due to the negative charges on the C═O groups that result in a strong electrostatic repulsion resulting in the anti isomer spontaneously.

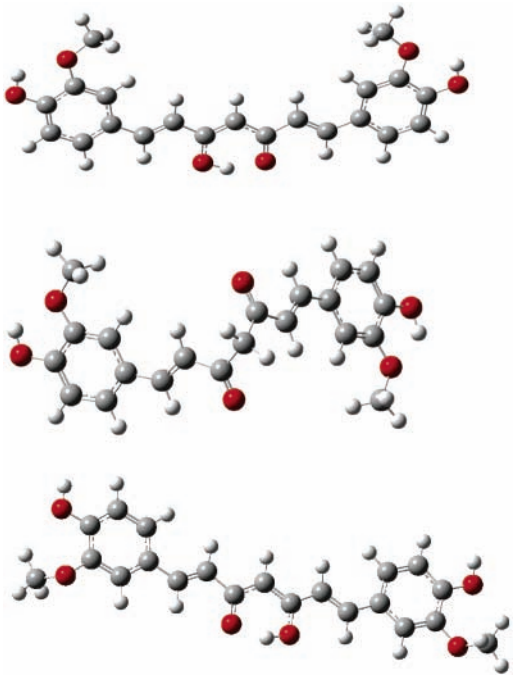

Figure 2. The final optimized structures of the enolic (first), anti-diketo (second) forms of curcumin as well as a higher-lying positional isomer (third) derived from the enolic structure (third). Note that the third structure is 11.8 kcal/mol higher than the syn-enol form as seen from **Table 1**.

Experimental studies of curcumin in solution (*18*, *35*) show that the enolic structure is favored in solution. For example, the ^1H and ^{13}C NMR and IR spectra (*35*) of curcumin in chlorobenzene, which is a low dielectric, reveal that the keto structure of curcumin undergoes a keto−enol rearrangement by transfer of proton from the $-CH_2$ group to form the enol structure shown in **Figure 1** (third structure). The keto−enol rearrangement is facilitated by the negative charges on the C═O groups and the reactive $-CH_2$ group next to it. Thus, the third structure shown in **Figure 1** was optimized fully in the 6311-G(2d,2p) basis at both DFT/B3LYP and MP2 levels of theory. The enolic form was definitely found to be the ground state and the most stable form in the gas-phase optimization of curcumin.

Several other structures that were depicted in the literature for curcumin have also been analyzed or optimized here. Sun et al. (*23*) have shown a series of structures in Figure 1 of their paper. The structures displayed in Figure 1 of Sun et al. have −OH groups in the meta or position 3 from the point of attachment of the aliphatic bridge to the ring and thus cannot be the correct structure of curcumin. In another structure considered by Sun et al. (*23*) the right side ring has the correct structure but the left benzene ring has −OH substituents in the incorrect position. The same comment applies to the enol structure in Figure 1 of Sun et al. (*23*), where the −OH groups are in positions 3 rather than the correct positions 4. The structures from the work of Zsila et al. (*5*) are correct relative to the positions of the −OH groups, but the $-OCH_3$ groups, even though they are in meta position, differ from **Figure 1** (structures). These structures and the optimized energies are considered here, but are found to be considerably higher than the structures shown in **Figure 1** both in solution and in vacuum.

Figure 2 shows the final optimized structures of the anti-diketo and enolic forms of curcumin and also a higher lying

Table 1. Computed Total Energies, Dipole Moments, and Relative Energies of Curcumin[a]

isomer	medium	total energy (hartree)	relative energy (kcal/mol)	dipole moment (D)	HOMO–LUMO (eV)
syn enol	gas phase	–1263.9639385	0	7.6655[b]	3.25
anti diketo	gas phase	–1263.9534178	6.7	0.8622	3.68
Figure 2, third structure	gas phase	–1263.9454528	11.8	6.7354	3.34
syn enol	aqueous solution	–1263.9946439	–19.5	10.77	3.07
anti diketo	aqueous solution	–1263.98374335	–12.6	1.41	3.52

[a] All energies were obtained at the optimized geometries in solution and gas phase using DFT/B3LYP and 6311-G(2d,2p) basis sets. [b] The dipole vector points predominantly along the *Y* direction with the actual vector components being (–0.4904, 7.6498, and 0.0005) at the DFT level and (–0.5532, 7.3763, and 0.0003) at the MP2 level, respectively.

isomer derived from the enolic structure. **Table 1** shows the computed energetics, dipole moments, relative energy separations, and HOMO−LUMO gaps of the three isomers of curcumin both in the gas phase and in solution. As can be seen from **Table 1**, the ground state both in the gas phase and in solution is the syn-enolic isomer shown in **Figure 2** (first structure). The diketo structure exists only in the anti form, and it is 6.7 and 6.9 kcal/mol above the enol form in the gas phase and solution, respectively. The structure considered by Zsila et al. (*5*) in the context of Cotton effects induced by binding of curcumin to HSA is 11.8 kcal/mol above the most stable enolic form shown in **Figure 2** (first structure). The differences between the two structures are in the relative positions of the methoxy ($-OCH_3$) groups, as be seen from the first and third structures of **Figure 2**.

With regard to the computed optimized geometries, because there are many parameters, only the most important parameters are discussed here. The C−O distance of the enolic C−OH is 1.326 Å in the gas phase, whereas the C═O bond involved in the cyclic hydrogen bond of the enol is 1.257 Å. Mague et al. (*36*) have reported the X-ray crystallographic data of a curcumin derivative recently. Their experimental C−O distance for the enolic C−OH is 1.306 Å, whereas the C═O distance of the group participating in the hydrogen bond is 1.274 Å. The computed phenolic −OH distance is 1.356 Å, and the C−OCH_3 distance is 1.371 Å. Hence, the enolic C−OH distance is shorter than the phenolic OH but longer than the C═O distance of the C═O group involved in the hydrogen bonding. The computed C−C distances in the aromatic ring are close to 1.38−1.39 Å, with only two of the distances near 1.41 Å. The computed aliphatic hydrocarbon bridge exhibits bond alternation with single bonds near 1.45 Å and double bonds near 1.346 Å, whereas the corresponding experimental values (*36*) are 1.457−1.469 for aliphatic single bonds and 1.327−1.384 Å for aliphatic double to alternation bonds. All computed bond angles near the enolic groups are within 0−1° of the reported experimental data (*36*). The only striking contrast is that the reported experimental hydrogen bond distance (*36*) for the enolic hydrogen bond is reported as 1.81 Å, whereas the computed gas-phase hydrogen bond distance is 1.608 Å at the MP2 level and 1.572 Å at the DFT level. In solution this bond length elongates a bit to 1.597 Å at the DFT level. Moreover O···H hydrogen bond distances are generally in the range computed here. Thus, the reported experimental data are somewhat longer, but in crystal structure this bond could be elongated compared to the gas-phase or aqueous solution. The bond angle for the hydrogen-bonded bridge agrees within less than a degree to the experiment (*36*). Likewise, the O···O distance of the enolic hydrogen-bonded moiety agrees well with experiment (*36*). In general, the optimized MP2 structure is quite close to the DFT structure except that the DFT method computes the O···H hydrogen bond distance shorter by 0.036 Å.

The anti-diketo structures have two C═O bonds with distances of 1.219 and 1.218 Å, respectively. The phenolic C−OH distances are 1.354 Å, and there are no substantial differences in the remaining bond lengths in comparison to the syn-enol form. A very important difference between the syn-enol form and the anti-diketo form is in the extent of planarity of the two halves of the conjugated framework. Whereas the syn-enol structure is planar with a dihedral angle of 180°, the anti-diketo structure exhibits considerable nonplanarity; that is, half of the structure is out of plane relative to the other half near the $-CH_2$ bridge with a dihedral angle of 73°. This feature is the same in aqueous solution also. The strong out-of-plane bending is caused by both the negative charges on the keto groups and the $-CH_2$ bridge group, which breaks the planarity in the case of the anti-diketo structure.

The optimized geometries in solution compared to the gas phase exhibited small differences in bond lengths and some differences in other geometrical parameters such as bond angles. The C−OH enolic distance in the solution is 1.333 Å, whereas the C═O distance of the group involved in the hydrogen bond is 1.267. These distances are elongated, somewhat more for the C═O in the solution. The phenolic C−OH distance is 1.353 Å, slightly shorter in the solution, whereas the aromatic ring distances change only in the third decimal point in the solution. In the aliphatic bridge only the C═C distance changes by 0.004 Å; the remaining changes are small or comparable. Even though the geometrical distances do not change significantly, the dipole moment of the syn-enol form in the solution is 10.77 D compared to the gas-phase value of 7.67 D; the large increase in the solution is thus ascribed to the charge transfer in solution and other stereochemical changes.

As seen from **Table 1**, the total energy stabilization of curcumin enolic form in water is 19.5 kcal/mol, whereas the anti-diketo form is stabilized by a comparable amount of 19.3 kcal/mol in relation to its gas-phase form.

The most important insight into the binding features of curcumin can be derived from the computed natural bond charges, which are shown for the isomers in the solution in **Figure 3**, noting that the gas-phase charges differ only in the second decimal compared to the solution. As can be seen from **Figure 3**, in both enolic and diketo forms curcumin exhibits polar groups at the end and middle and an essentially hydrophobic aliphatic bridge connecting them. The enolic O charges are near −0.7, very close to the phenolic O charge of −0.7. In the anti-diketone isomer the charges on the oxygens are −0.6, still quite negative, and presumably the negative charge is even larger in the syn structure, which leads to the repulsion of the C═O groups, resulting in the anti structure. Note that in the diketo form the hydrogens are positively charged, particularly the $-CH_2$ bridge, whereas the hydrogens of the enolic form are nearly neutral.

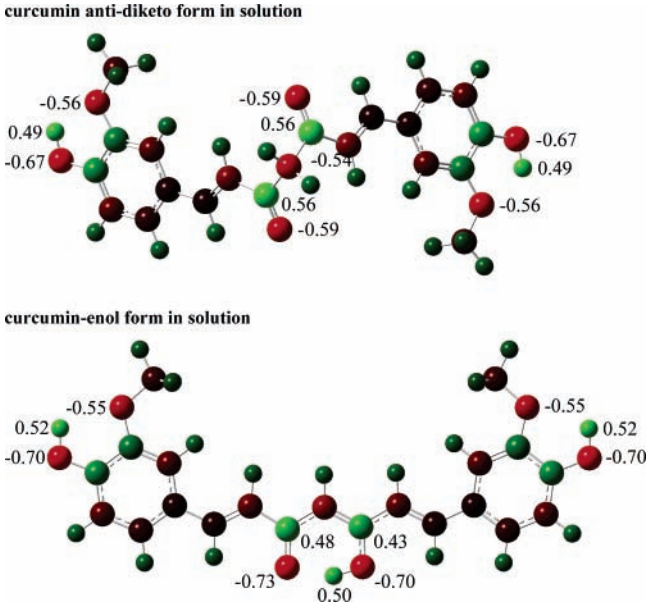

Figure 3. Natural bond charges computed for the enol and anti-diketo isomers of curcumin in aqueous solution. Note that the red color means the atoms are negatively charged, green indicates positive charge, whereas black and near-black colors indicate the atoms are nearly neutral. This figure shows that curcumin has polar end and middle groups separated by a hydrophobic conjugated carbon bridge.

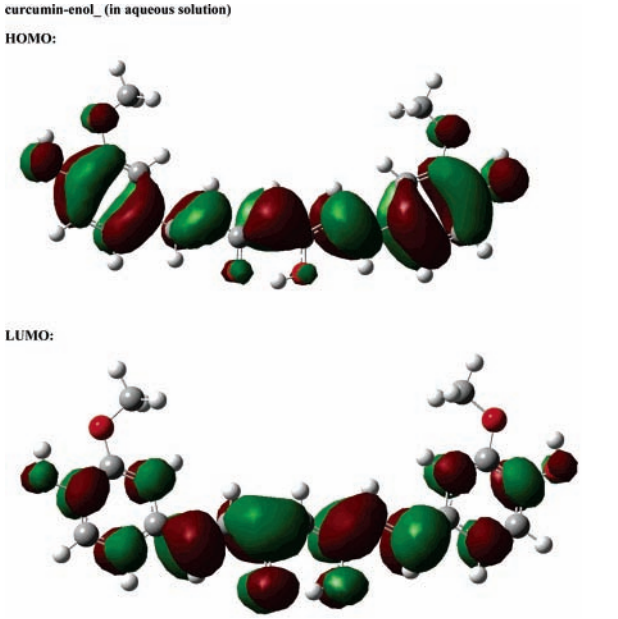

Figure 4. HOMO and LUMO plots of curcumin. The orbitals show considerable delocalization over the entire framework in both LUMO and HOMO.

As seen from the color charge maps in **Figure 3**, curcumin is quite interesting in possessing highly polar enolic and phenolic groups separated by an aliphatic bridge, which is hydrophobic in nature. The overall large dipole moment of 10.77 D confirms the polar ends and the middle group of curcumin in the enolic form. As noted by Fujisawa et al. (*15*) the experimentally observed hydrophobicity of curcumin is log $P = 2.5$. The observed level of hydrophobicity of curcumin is consistent with the computed features of a predominantly hydrophobic bridge of curcumin as seen from **Figure 3**. It should be noted that the polar groups at the end and middle should weaken the hydrophobic feature, and yet the fact that the overall log P value is 2.5 for curcumin is suggestive of a highly hydrophobic bridge of curcumin.

It is the strongly hydrophobic aliphatic bridge that facilitates curcumin's penetration into the blood−brain barrier. Once curcumin penetrates the barrier, there are two mechanisms by which curcumin prevents AD. The first possibility is that the polar groups bind to β-amyloid, which is responsible for the formation of the plaque and degeneration of the brain cells. The other possibility is that the highly polar $C-O^-$ groups near the center of the curcumin molecule may bind to metal ions such as Fe and Cu through chelation similar to six-membered rings formed in the enolic form of curcumin. The computed charges and geometrical features do not eliminate either possibility, and thus curcumin may be actively binding to β-amyloid and also removing the metal ions through a chelation process. It has been suggested that curcumin binds to the peptide sequences that form fibrils or protofibrils by Cole and co-workers (*1*). A few sequences that have been identified by Cole and co-workers (*1*) are Aβ 12−28 and 25−35, which have the ability to form fibrils, and curcumin was found to stain them. It has also been suggested that curcumin does not bind to the monomeric form for Aβ but to a secondary oligomeric structure involved later in the process. In any case, the binding should be assisted by the C−O groups through hydrogen bonding to the peptide sites.

Further insight can be derived from the binding features of curcumin by analyzing the frontier orbitals of curcumin. **Figure 4** shows the highest occupied molecular orbital (HOMO) and lowest unoccupied molecular orbital (LUMO) of curcumin in the enolic form. There is not much difference in the HOMO and LUMO for the gas-phase structure and the ones in solution. As seen from **Figure 4**, the HOMO is much delocalized over the entire structure in a π molecular orbital and involves bonding combination at the enolic-keto cycle and delocalized antibonding over the conjugated framework. Interestingly, even the oxygens of the two $-OCH_3$ methoxy groups are slightly involved in the HOMO. The LUMO, which is predominantly π^* in character, as seen from **Figure 4**, involves alternating opposite signs including the enolic-keto bridge. The LUMO does not involve the $-OCH_3$ groups, as expected.

On the basis of the HOMO and LUMO analysis it can be concluded that the binding between curcumin and the Aβ oligomer is assisted by electron transfer from the π HOMO orbital shown in **Figure 4** to the Aβ oligomer followed by back charge transfer from the oligomer to the π^* antibonding orbital LUMO, shown in **Figure 4**. The same mechanism of bonding and back-bonding should be involved in binding with Cu and Fe ions and curcumin. The strong negative charges at the enolic-keto bridge should be the entities that should provide the required charge to the peptide binding sites or the metal ion, and back transfer of charge will be accepted by the LUMO of curcumin.

Laplacian is the second gradient of the charge density and can provide very sharp contrasting features, especially concerning the positive charges as peaks on a molecule as complex as curcumin. Because the NBO analysis provided the various charges, the Laplacians can provide complementary information. Thus, it was decided to investigate and compute the Laplacian of the charge density of curcumin, which is shown in **Figure 5**. As can be seen from **Figure 5**, there are a number of peaks in the Laplacian of curcumin. The peaks in the Laplacian are regions of electron deficiency or electrophilic regions on the molecule. It can be seen that there are such regions present throughout the structure, which means curcumin can not only donate electronic charge through the enolic group but also

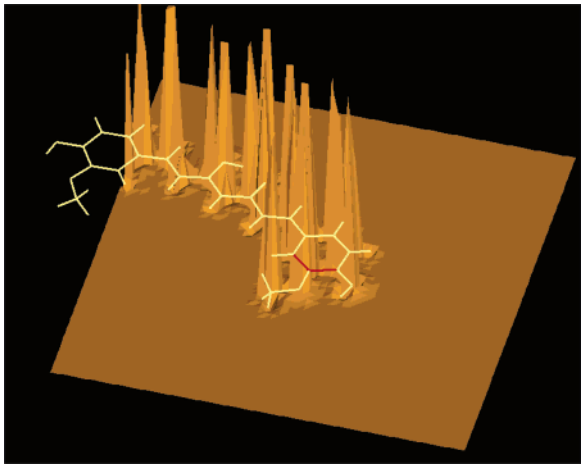

Figure 5. Laplacian plot of the curcumin enolic structure. Laplacian is the second gradient of the charge density, which shows several peaks over the entire structure. The peaks are the electrophilic regions of the molecule, which suggest that the electronic charge received by curcumin from a protein or Aβ oligomer will be delocalized over the whole structure.

Table 2. Adiabatic Ionization Energy and Electron Affinity of Curcumin(enol)

species	total energy (hartree)	relative *E* (eV)	state
neutral curcumin	–1263.9639385	0.0	singlet
curcumin anion	–1264.0059722	–1.14 EA = 1.14	doublet
curcumin cation	–1263.7226259	6.57 IP = 6.57	doublet

receive electronic transfer through the LUMO at electrophilic regions represented by the various peaks of the Laplacian in **Figure 5**. It can be seen that there are multiple peaks in **Figure 5**, which are consistent with the delocalized nature of the LUMO. This suggests the strong propensity of curcumin to have the received electronic charge from a binding site delocalized over the conjugated network.

The adiabatic ionization energy and electron affinity of curcumin in the enolic form have also been computed. The computed results are shown in **Table 2**. As seen from this table, curcumin has an electron affinity of 1.14 eV at the DFT level, which is consistent with the characteristics of its Lapalcian and LUMO both pointing to a delocalized electrophilic feature. The adiabatic ionization potential is defined as the difference between the total energy of the neutral species at its optimized geometry minus the total energy of the cation at its optimized energy. This value, as seen from **Table 2**, is 6.57 eV. Two insightful properties that can be derived from these results are the chemical potential and molecular hardness, which are $-(IP + EA)/2$ and $(IP - EA)/2$, respectively. The computed results indicate that curcumin has a chemical potential of -3.86 eV and a molecular hardness of 2.72 eV. The molecular hardness is a more useful number than just the HOMO−LUMO gap, which comes out to be 3.25 eV for the curcumin-enol form. It is generally believed that the chemical potential measures the escaping tendency of electrons from the molecule, and it is then related to the electronic charge rearrangement, whereas the molecular hardness is a resistance to the charge transfer or reactivity. Higher hardness means less reactivity or more stability. Consequently, curcumin has a reasonable propensity to both donate its highest occupied electron and receive electron density, thus explaining its binding features to both β amyloid and metal ions. It should be pointed out that the syn structure is more suitable for curcumin to bind to metal ions as the diketo groups can chelate to the metal ions forming a ring structure, analogous to the enol form of curcumin.

The low molecular hardness of 2.72 eV is consistent with the instability of curcumin above neutral pH. As discussed by the author (*20*, *21*) the yellow color of curcumin is attributed to a blue n−π* transition, which exhibits λ_{max} at 420 nm, explaining the yellow color. However, the color of turmeric varies dramatically in different media, and the author (*20*, *21*) has provided the mechanism for color change from yellow to red upon addition of OH^- to a neutral solution of curcumin. It was shown by the author (*20*) that curcumin readily donates a proton from its phenolic −OH group and forms an anion upon addition of OH^-, and it was shown that the formation of the anion results in a delocalized excitonic quinonoid state, which causes the red shift to the n−π* transition. There has been some discussion in the literature if enolic −OH would be the proton donor (*16*), but a more recent experimental study (*35*) asserts that it is the phenolic −OH which donates the proton, consistent with the author's proposed mechanism (*20*) for proton donation. The anion undergoes extension of conjugation, resulting in a red shift in the observed spectra and, thus, the red color of turmeric in alkaline media. That is, curcumin reacts with nucleophiles primarily though the donation of H^+ from phenolic −OH and then undergoes charge delocalization due to the conjugated network. Its reacts with electrophilic species such as metal ions through the diketone group, which is electron-rich, but, again, as seen from the Laplacian in **Figure 5**, there is considerable delocalization of reaction with electrophiles.

As mentioned under Computational Methods, computationally intensive MP2 geometry optimizations of the curcumin-enol isomer have also been carried out. Thus, it would be interesting to compare the MP2 results with the DFT/B3LYP results. The main contrast between the two methods is in the representation of the hydrogen bonding at the enolic ring structure. The O- - -H hydrogen bonding distance at the DFT level is 1.572 Å, wheres the corresponding distance at the MP2 level is 1.609 Å; consequently, the DFT method predicts too short a distance for the O···H hydrogen bonding distance. This is understandable in view of the fact that dispersion interactions are not included in the DFT/B3LYP method, and thus the hydrogen bonding is not properly represented in the DFT/B3LYP method. Otherwise, the two methods exhibit an overall agreement with respect to the geometries. For example, some of the vital bond parameters could be compared. The MP2 enolic C−OH distance is 1.332 Å, whereas the C═O distance hydrogen-bonded to the enolic group is 1.255 Å; these values compare with DFT results of 1.326 and 1.257 Å, respectively. The phenolic C−OH distance is 1.360 Å, whereas the C−OCH_3 distance is 1.370 Å at the MP2 level. The corresponding values at the DFT level are 1.356 Å for the phenolic C−OH and 1.371 Å for the C−OCH_3 distance, respectively. The differences in the C−C distances between the MP2 and DFT levels were between 0.0007 and 0.006 Å. Consequently, it is concluded that the differences are quite small relative to the geometric distances between the two methods. It is concluded that the hydrogen bonding is not properly described by the DFT method. The differences in the geometries found near the polar groups are also consistent with the differences in the charges between the MP2 and DFT levels. The DFT method tends to produce greater charge separations compared to the MP2 method. For example, the MP2 C−O charges for the phenolic groups are −0.560 for the oxygen, whereas they are −0.67 at the DFT level. Likewise, the enolic

C—O groups' oxygen charges are −0.58 and −0.68 at the MP2 and DFT levels, respectively. The total dipole moment at the MP2 level is 7.2247 D compared to the DFT dipole moment of 7.67 D; thus, the DFT method produces more charge separation compared to the MP2 method. The overall dipole vector predominantly points in the *Y* direction.

It is noted that there have been previous computations (*5*, *20*, *23*) on species related to curcumin. As mentioned before, unfortunately, some of these works do not treat the curcumin molecule in its correct lowest isomeric form. The work of Zsila et al. (*5*) and Wright (*22*) have considered an isomer of curcumin that has the $-OCH_3$ groups in non-meta positions. These structures have $-OCH_3$ groups in positions different from the minimum energy structures shown in **Figures 1** and **3** (first two structures). The work of Sun et al. (*23*) mentions two structures in Figure 1 of their work, but these structures do not have phenolic −OH groups in the para (fourth) position and thus cannot represent the true structures of curcumin. However, Sun et al. (*23*) show the correct three-dimensional structure of curcumin for the enolic form in Figure 2 of their paper. The basis set employed by Sun et al. is smaller than the one used here for geometry optimization, but they did a final single-point computation with the same basis set as the one used here. This may explain why their total energies are higher than the ones reported in **Table 1** of this work.

The predicted binding sites and binding features of curcumin are very critical to the understanding of not only AD but also how curcumin binds to human proteins such as human serum albumin (HSA). Zsila et al. (*5*) have carried out circular dichroism (CD) studies of curcumin binding to HSA. The isomer for curcumin that they have considered is higher in energy (see **Table 1**) in that the $-OCH_3$ groups are on the enolic side in their structure, whereas in the lowest optimized structure the same group is on the other side. It is expected that the observed spectral features would not to be altered by this variation of the positions of $-OCH_3$ groups because the chromophores do not involve the OCH_3 groups. Zsila et al. (*5*) have concluded that the primary binding site to HSA-protein is site I of HSA, which could be called HSA-I. As seen from the computations, the hardness of curcumin is only 2.72 eV, which implies that curcumin is softly acidic and ready to react with alkaline binding sites or undergo phenolic dissociation by yielding H^+ and the deprotonated anion. As can be inferred from the Laplacian plot shown in **Figure 5**, there is a sharp peak near the phenolic −OH reflecting depletion of electronic charge density on the proton. Moreover, the Mulliken charges on the phenolic −OH group also suggest that the phenolic −OH groups are quite acidic due to the delocalization of charge density seen in **Figure 5**. Thus, dissociation of the phenolic −OH group to yield H^+ and the formation of the curcumin anion are both critical to the binding to HSA-I and also the β-amyloid that causes plaque, resulting in AD. Once the anion is formed, there is considerable resonance of charge density from one end of the ring to the other, resulting in the extension of conjugation and intermolecular exciton coupling between the two chromophore parts of curcumin. This results in a quinonoid structure and extension of conjugation in conformity with the observed red shift. There is some uncertainty (*5*) if the pK_a for the enolic −OH should be near pH 7.4, but the phenolic OH pK_a value is near 8.2.

Zsila et al. (*5*) have suggested that acidic dissociation of curcumin influences its binding to the HSA protein. This is the key mechanism for binding of curcumin to HSA-I. The deprotonated anionic form of curcumin could facilitate strong hydrogen bonding with basic residues of HSA and other proteins. According to the CD spectral evidence (*5*), the curcumin binding to the HSA-I site results in a chiral configuration where the two parts of curcumin fold into configuration with a dihedral angle of 156°. This chiral feature induces CD as a result of intermolecular chiral exciton coupling of the two parts of the curcumin molecule, referred to as ferulyl chromophores. The excitonic feature of this interaction is due to the delocalization of the electronic charge over the entire structure, consistent with its LUMO shown in **Figure 4** and also the Laplacian shown in **Figure 5**. The current author (*20*) has previously proposed a mechanism for the observed bathochromic red shift of curcumin in alkaline media at pH >8. This mechanism of charge resonance throughout the conjugated network results in a delocalized quinonoid-type of structure for curcumin resulting in a large bathochromic shift due to increase in pH. Zsila et al. (*5*) have found a similar red shift in the HSA-bound curcumin spectra. The observed red shift in such spectra substantiates the fact that the protein-bound curcumin is in a deprotonated anionic form that is stabilized by excitonic interaction and through the hydrogen bonding to the protein. This is indicative of the dissociation of the phenolic proton and formation of the delocalized curcumin anion that is hydrogen-bonded to the protein.

On the basis of both the computed results and the CD spectra (*5*) of curcumin bound to the HSA protein, it is suggested that once curcumin binds to an Aβ oligomer, the complex would be quite stable in a hydrophobic cavity, and thus decomposition of free curcumin in aqueous medium is not feasible. Such hydrophobic cavities are found in protein-binding sites, which could assist in the stabilization of the curcumin complex. The fact that curcumin is not charged and contains a hydrophobic bridge assists its penetration through the blood−brain barrier. It is not clear if deprotonation is a prerequisite for curcumin to bind to Aβ amyloid. This has been suggested to be the primary mechanism for proteins such as HSA followed by hydrogen bonding of the anion to the protein.

In conclusion, several isomers of curcumin have been studied here, and it is found that the syn-enol form and the anti-diketo form and another syn-enolic isomer are all minima with real vibrational frequencies. Among the isomers considered here, the syn-enolic form was found to be most stable in both gas phase and aqueous solution. The syn-enolic form exhibits very large dipole moments of 10.77 D in aqueous solution and 7.67 D in the gas phase or vacuum. The syn-enolic framework is planar, whereas the anti-diketo structure exhibits a folded structure strongly deviating from a planar structure with a dihedral angle of 73°.

The computed HOMO−LUMO gap and the ionization potential and electron affinity values confirm that curcumin exhibits low hardness and thus a tendency to readily deprotonate to form curcumin deprotonated anion, which is stabilized by extension of conjugation. The analysis of natural bond charges reveals that the enolic and phenolic groups are quite polar, separated by a nearly neutral hydrophobic conjugated hydrocarbon bridge. Thus, the hydrocarbon bridge facilitates penetration into the blood−brain barrier, a key preceding mechanism for curcumin's binding to amyloid-β oligomers in the brain cell. The polar groups and particularly the phenolic and enolic −OH groups provide for a channel of deprotonation and subsequent binding of the resulting anionic species to the protein binding sites through hydrogen bonding. It has been demonstrated here through the analysis of HOMO, LUMO, and Laplacians of the charge density that the charge is considerably delocalized, providing for resonance stabilization following binding to the

HSA-I site of the protein. This explained the observed chiral intermolecular excitonic coupling in the CD spectra of HSA-I-bound curcumin. The chirality is caused by the binding of curcumin to protein sites through hydrogen bonding, and curcumin deprotonation was proposed to be an important step that facilitates subsequent binding through delocalization of the charge and stabilization. The hydrogen bonding between curcumin and protein are important and assisted by the charge delocalization. The computed low molecular hardness of curcumin indicates its propensity to deprotonate and is consistent with the observed CD spectra of Zsila et al. (*5*). A qualitative explanation through charge analysis, HOMO, LUMO, and Laplacian was provided here to understand the features of curcumin that facilitate Aβ binding and curcumin's preventive and curing property of AD observed by Cole and co-workers (*1*). There are many questions that remain unanswered. For example, is chelation of curcumin with metal ions important for AD prevention? What is the precise structure of the curcumin−Aβ oligomer complex? Can other molecules be designed through molecular similarity and drug design analysis that are better drugs comparable to curcumin for preventing or curing AD? These are the types of questions that could be the topic of future investigations.

LITERATURE CITED

(1) Yang, F.; Lim, G. P.; Begum, A. N.; Ubeda, O. J.; Simmons, M. R.; Ambegaokar, S. S.; Chen, P.; Kayed, R.; Glabe, C. G. Frautschy, S. A.; Cole, G. M. Curcumin inhibits formation of amyloid β oligomers and fibrils, binds plaques, and reduces amyloid in vivo. *J. Biol. Chem.* **2004**, *280*, 5892−5901.

(2) Weggen, S.; Eriksen, J. L.; Das, P.; Sagi, S. A.; Wang, R.; Pietrizik, C. U.; Findlay, K. A.; Smith, T. E.; Murphy, M. P.; Butler, T.; Kang, D. E.; Marquez-Sterling, N.; Golde, T. E.; Koo, E. H. A subset of NSAIDs lower amyloidogenic Aβ 42 independently of cyclooxygenase activity. *Nature* **2001**, *414*, 212−216.

(3) Gasparini, L.; Rusconi, L.; Xu, H.; del Soldato, P.; Ongini, E. Modulation of β-amyloid metabolism by non-steroidal anti-inflammatory drugs in neuronal cell cultures. *J. Neurochem.* **2004**, *88*, 337−348.

(4) Lim, G. P.; Chiu, T.; Yang, F.; Beech, W.; Frautschy, S. A.; Cole, G. M. The curry spice curcumin reduces oxidative damage and amyloid pathology in an Alzheimer transgenic mouse *J. Neurosci.* **2001**, *21*, 8370−8377.

(5) Zsila, F.; Bikádi, Z.; Simonyi, M. Molecular basis of Cotton effects induced by the binding of curcumin to human serum albumin. *Tetrahedron: Asymmetry* **2003**, *14*, 2433−2444.

(6) Rovner, S. L. Untangling Alzheimer's—cover story. *Chem. Eng. News* **2005**, *83* (8, Feb 21), 38−45.

(7) Masuda, T.; Toi, Y.; Bando, H.; Maekawa, T.; Takeda, Y.; Yamaguchi, H. Structural identification of new curcumin dimers and their contribution to the antioxidant mechanism of curcumin. *J. Agric. Food Chem.* **2002**, *50*, 2524−2530.

(8) Woo, J.; Kim, Y.; Choi, Y.; Kim, D.; Lee, K.; Bae, J. H.; Min, D. S.; Chang, J. S.; Jeong, Y. J.; Lee, Y. H.; Park, J.; Kwon, T. K. Molecular mechanisms of curcumin-induced cyclotoxicity: induction of apoptosis through generation of reactive oxygen species, down-regulation of Bcl-X_L and IAP, the release of cytochrome *c* and inhibition of Akt. *Carcinogenesis* **2003**, *24*, 1199−1208.

(9) Moos, P. J.; Edes, K.; Mullally, J.; Fitzpatrick, J. Curcumin impairs tumor suppressor p53 function in colon cancer cells. *Carcinogenesis* **2004**, *9*, 1611−1617.

(10) Rashmi, R.; Kumar, S.; Karunagaran, D. Human colon cancer cells lacking Bax resisit curcumin-induced apoptosis and Bax requirement is dispensable with ectopic expression of Smac or downregulation of Bcl-Xl. *Carcinogenisis* **2005**, *26*, 713−723.

(11) Khafif, A.; Schantz, S. P.; Chou, T. C.; Edelstein, D.; Sacks, P. G. Quantification of chemopreventive synergism between (−)-epigallocatechin-3-gallate and curcumin in normal, premaligannat and malignant human oral epithelial cells. *Carcinogenisis* **1998**, *19*, 419−424.

(12) Balasubramanian, S.; Eckert, R. Green tea polyphenol snd curcumin inversely regulate human involucrin promoter activity via opposing effects on CCAAT/enhancer-binding protein function. *J. Biol. Chem.* **2004**, *23*, 24007−24014.

(13) Van Erk, M. J.; Teuling, E.; Staal, Y. C. M.; Huybers, S.; van Bladeren, P. J.; Aarts, J. M. M. J. G.; van Ommen, B. Time- and dose-dependent effects of curcumin on gene expressio in human colon cancel cells *J. Carcinogen.* **2004**, *3*, 1−17.

(14) Kim, M.-k.; Choi, G.-j.; Lee, H.-s. Fungicidal property of *Curcuma longa* L. rhizome-derived curcumin against phytopathogenic fungi in a greenhouse. *J. Agric. Food Chem.* **2003**, *51*, 1578−1581.

(15) Fujisawa, S.; Atsumi, T.; Ishihara, M.; Kadoma, Y. Cyctotoxicity, ROS generation activity and radical-scavengining activity of curcumin and related compounds. *Anticancer Res.* **2004**, *24*, 563−569.

(16) Jovanovic, S. V.; Steenken, S.; Boone, C. W.; Simic, M. G. H−atom transfer is a preferred antioxidant mechanism of curcumin. *J. Am. Chem. Soc.* **1999**, *121*, 9677−9681.

(17) Zsila, F.; Bikádi, Z.; Simonyi, M. Unique, pH-dependent biphasic band shape of the visible circular dichroism of curcumin-serum albumin complex. *Biochem. Biophys. Res. Commun.* **2003**, *301*, 776−872.

(18) Khopde, S. M.; Priyadharshini, K. I.; Palit, D. K.; Mukherjee, T. Effect of solvent on the excited-state photophysical properties of curcumin. *Photochem. Photobiol.* **2000**, *72*, 625−631.

(19) Borsari, M.; Ferrari, E.; Grandi, R.; Saladani, M. Curcuminoids as potential new iron-chelating agents: spectroscopic, polarographic and potentiometric study on their Fe(III) complexing ability. *Inorg. Chim. Acta* **2002**, *328*, 61−68.

(20) Balasubramanian, K. Two colorful applications of the PPP method. *Int. J. Quantum Chem.* **1990**, *37*, 449−464.

(21) Balasubramanian, K. Theoretical calculations on the UV−visible spectra of the curcumin pigment in turmeric. *Indian J. Chem.* **1991**, *30A*, 61−65.

(22) Wright, J. S. Predicting the antioxidant activity of curcumin and curcuminoids**.** *J. Mol. Struct. (THEOCHEM)* **2002**, *591*, 207−217.

(23) Sun, Y. M.; Wang, R. X.; Yuan, S. L.; Lin, X. J.; Liu, C. B. Theoretical study of the antioxidant activity of curcumin. *Chinese J. Chem.* **2004**, *22*, 827−830.

(24) Mazumder, A.; Neamati, N.; Sunder, S.; SchuLz, J.; Perez, H.; Eich, E.; Pommier, Y. Curcumin analogs with altered potencies against HIV-1 integrase as probes for biochemical mechanisms of drug action. *J. Med. Chem.* **1997**, *40*, 3057−3063.

(25) Basak, S. C. Use of molecular complexity indices in predictive pharmacology and toxicology: a QSAR approach. *Med. Sci. Res.* **1987**, *15*, 605−640.

(26) Basak, S. C.; Mills, D.; Gute, B. D.; Hawkins, D. Predicting mutagenicity of congeneric and diverse sets of chemicals using computed molecular descriptors: a hierarchical approach. *Quantitative Structure−Activity Relationship (QSAR) Models of Mutagens and Carcinogens*; Benigni, R., Ed.; CRC Press: Boca Raton, FL, 2003; Chapter 7, pp 207−234.

(27) Dias, J. R *Handbook of Polycyclic Aromatic Hydrocarbons*; Elsevier: Amsterdam, The Netherlands, 1987.

(28) Parr, R. G.; Yang, W. *Density Functional Theory of Atoms and Molecules*; Oxford University Press: New York, 1989.

(29) Møller, C.; Plesset, M. S. Note on an approximation treatment for many-electron systems. *Phys. Rev.* **1934**, *46*, 618−622.

(30) Becke, A. D. Density-functional thermochemistry. III. The role of exact exchange. *J. Chem. Phys.* **1993**, *98*, 5648−5652.

(31) Cances, E.; Mennucci, B.; Tomasi, J. A new integral equation formalism for the polarizable continuum model: theoretical background and applications to isotropic and anisotropic dielectrics *J. Chem. Phys.* **1997**, *107*, 3032−3041.

(32) Mennucci, B.; Cances, E.; Tomasi, J. Evaluation of solvent effects in isotropic and anisotropic dielectrics and in ionic solutions with a unified integral equation method: theoretical bases, computational implementation, and numerical applications. *J. Phys. Chem. B* **1997**, *101*, 10506−10517.

(33) Mennucci, B.; Tomasi, J. Continuum solvation models: A new approach to the problem of solute's charge distribution and cavity boundaries. *J. Chem. Phys.* **1997**, *106*, 5151−5158.

(34) Frisch, M. J.; Trucks, G. W.; Schlegel, H. B.; Scuseria, G. E.; Robb, M. A.; Cheeseman, J. R.; Zakrzewski, V. G.; Montgomery, J. A., Jr.; Stratmann, R. E.; Burant, J. C.; Dapprich, S.; Millam, J. M.; Daniels, A. D.; Kudin, K. N.; Strain, M. C.; Farkas, O.; Tomasi, J.; Barone, V.; Cossi, M.; Cammi, R.; Mennucci, B.; Pomelli, C.; Adamo, C.; Clifford, S,; Ochterski, J.; Petersson, G. A.; Ayala, P. Y.; Cui, Q.; Morokuma, K.; Salvador, P.; Dannenberg, J. J.; Malick, D. K.; Rabuck, A. D.; Raghavachari, K.; Foresman, J. B.; Cioslowski, J.; Ortiz, J. V.; Baboul, A. G.; Stefanov, B. B; Liu, G.; Liashenko, A.; Piskorz, P.; Komaromi, I.; Gomperts, R.; Martin, R. L.; Fox, D. J.; Keith, T.; Al-Laham, M. A.; Peng, C. Y.; Nanayakkara, A.; Challacombe, M.; Gill, P. M. W.; Johnson, B.; Chen, W.; Wong, M. W.; Andres, J. L.; Gonzalez, C.; Head-Gordon, M.; Replogle, E. S.; Pople, J. A. *Gaussian 03*, revision C.02; Gaussian, Inc.: Pittsburgh, PA, 2005.

(35) Barclay, L. R. C.; Vinquist, M. R.; Mukai, K.; Goto, H.; Hashimoto, Y.; Tokunaga, A.; Uno, H. On the antioxidant mechanism of curcumin: classical methods are needed to determine antioxidant mechanism and activity. *Org. Lett.* **2000**, *2*, 2841−2843.

(36) Mauge, J. T.; Alworth, W. L.; Payton, F. L. Curcumin and derivatives. *Acta Crystallogr.* **2004**, *C60*, 608−610.

Received for review February 6, 2006. Revised manuscript received March 16, 2006. Accepted March 20, 2006. The work at Lawrence Livermore National Laboratory was performed in part under the auspices of the U.S. Department of Energy by the University of California, LLNL, under Contract W-7405-Eng-48. Research at California State University, East Bay, was supported by the National Science Foundation under Grant CHE-0236434. Computations were performed on LLNL's accelerated supercomputing initiative's (ASCI) uv machine, which consists of 992 IBM SP4 processors as well as a server with 4 Intel IA-64 processors.

JF0603533